Comparison of frequency domain measures based on spectral decomposition for spontaneous baroreflex sensitivity assessment after Acute Myocardial Infarction

Riccardo Pernice[a,,§], Laura Sparacino[a,§], Giandomenico Nollo[b], Alessandro Busacca[a], Luca Faes[a]*

[a]*Department of Engineering, University of Palermo, 90128 Palermo, Italy*
[b]*Department of Industrial Engineering, University of Trento, 38123 Trento, Italy*
[*]riccardo.pernice@unipa.it
[§]These authors contributed equally to this work

Abstract

The **objective** of this study is to test the hypothesis that the baroreflex control of arterial pressure is altered after acute myocardial infarction (AMI) comparing different approaches for its evaluation based on the spectral analysis of spontaneous systolic arterial pressure (SAP) and heart period (HP) variability. We present a new **method** to assess directed interactions between SAP and RR from their linear model representation, based on pole decomposition of the model transfer function and evaluation of causal measures of coupling and gain from the poles associated to low frequency (0.04-0.15 Hz) oscillatory components. The method was compared with traditional non-causal approaches for the spectral analysis of the baroreflex gain, and with causal approaches based on the directed coherence, in a group of AMI patients and in Young and Old healthy controls studied at rest and during head-up tilt. Analysis of feedforward interactions from RR to SAP was also performed. Our **results** support the importance of using causal approaches to quantify separately baroreflex and feedforward interactions between RR and SAP. In AMI patients, these approaches revealed lower coupling and gain from SAP to RR, suggesting weaker effectiveness and lower sensitivity of the baroreflex after infarction, while they did not indicate clear alterations in the response to tilt. The postural stress altered instead the feedforward interactions selectively across groups, being related to decreased coupling only in Young and to increased gain mostly in AMI. These results have **significance** for the clinical assessment of the baroreflex and the physiological evaluation of cardiovascular interactions.

Keywords: spectral decomposition, frequency domain, causality, baroreflex, head-up tilt, cardiovascular control, acute myocardial infarction

2010 MSC: 92C55, 92C30

1. Introduction

The baroreflex mechanism has a key role in the short-term regulation of systolic arterial pressure (SAP) and heart period (measured as the RR interval of the electrocardiogram, ECG), which are known to dynamically interact in a closed loop, as a consequence of the baroreflex feedback of SAP on RR and of feedforward pathways of mechanical nature, whereby SAP is influenced by previous RR changes [1,2]. The baroreflex represents a fundamental mechanism to maintain the optimal blood pressure level continuously or in response to changing physiological conditions, and accomplishes to such a task modulating the heart rate [3–6]. Specifically, a decrease in arterial blood pressure evokes a baroreflex response leading to an increased heart rate, while an increase in arterial blood pressure is followed by the opposite effect. While in healthy subjects the baroreflex acts in response to physiological stressors such as change of posture, mental workload and others, an impairment of baroreflex control is thought to be often associated with age, orthostatic intolerance and pathologies like heart failure or acute myocardial infarction (AMI), as postural circulatory stress and cardiovascular diseases elicit baroreceptor unloading [7–10]. Therefore, assessment of the baroreflex sensitivity (BRS), often evaluated from the spontaneous beat-to-beat fluctuations of RR and SAP as the magnitude of the reflex change in RR corresponding to a unitary change in SAP, can provide valuable information for the analysis of cardiovascular regulation in normal and pathological conditions and can have an important diagnostic and clinical value [4,11,12]. An appropriate evaluation of the BRS should take into account not only the oscillatory nature of cardiovascular parameters, being able to separate contributions occurring in different frequency bands - typically divided into very low-frequency (VLF, up to 0.04 Hz), low-frequency (LF, 0.04 – 0.15 Hz) and high-frequency (HF, 0.15– 0.4 Hz) bands- but also the closed-loop nature of cardiovascular interactions [13]. Usually, the frequency analysis of feedback baroreflex interactions is carried out focusing on the LF band to avoid the confounding effects of other variables operating at different frequencies (e.g., respiration) and causal analysis methods are adopted to minimize the effect of non-baroreflex mechanisms on the BRS estimates [14–18]. On the other hand, though much less investigated, the feedforward mechanism from RR to SAP is also important in the assessment of the balanced cardiovascular regulation in normal and diseased conditions [7].

The directed (causal) coherence (DC) has been proposed and used as a linear frequency domain measure of causal interactions between coupled dynamic processes [11,19]. The DC from a source to a target process is computed from the spectral representation of their descriptive vector autoregressive (AR) model, whose parameters provide the basis to separate the power spectral density (PSD) of the target process into partial spectra related to its own dynamics and to the dynamics of the source process. As in practical applications both the DC function and baroreflex gain need to be quantified in specific frequency regions, empirical approaches are generally adopted. They consist in taking the maximum or average value, within the band of interest, of the analyzed spectral function. However, these approaches often lead to ambiguous choices (a maximum value can be absent within the observed band) or imprecise quantifications (the average value may be affected by spectral effects of nearby broadband oscillations) [11].

To overcome these limitations, the present study introduces a modification of the causal coherence and of the previous definitions of spectral baroreflex gain [10,20] based on the spectral decomposition method [21]. Specifically, spectral decomposition is applied to the partial spectra of the PSD of the target process, representing each partial spectrum as the sum of bell-shaped functions with features (power, frequency, spectral bandwidth) related to the type and location (modulus and phase) of the poles of the transfer function which defines the vector AR process in the Z-domain. Then, the power content associated to the decomposed spectral components with frequency inside the band of interest (here, the LF band) is elaborated to obtain pole-specific measures of coupling and gain within the band. These measures, which we refer to as "local" due to their frequency-specific nature, are compared in the present work with the corresponding "global" measures obtained as the band-averaged DC and gains. The analysis, also extended to the comparison between causal and non-causal measures of gain and to the quantification of feedforward (non-baroreflex) interactions, is performed on the joint variability series of the heart period and the systolic arterial pressure measured in a group of post-AMI patients monitored at rest and during orthostatic stress, as well as in two control groups of healthy subjects (younger and age-matched with AMI). Preliminary methodological and applicative results have been presented in a reduced form in conference contributions [13], [22].

2. Methods

2.1 Measures of causal coupling and gain derived from parametric cross-spectral analysis

Let us consider a bivariate stochastic process Y composed by two jointly stationary, zero mean discrete stochastic processes y_1 and y_2. Defining $Y(n) = [y_1(n)\ y_2(n)]^T$ as the vector variable sampling the process at time $t_n = nT_s$, where T_s is the sampling period, it is possible to express the causal interactions occurring between the processes in a parametric form through a *p*-order bivariate autoregressive (AR) model as follows [22–24]

$$Y(n) = \sum_{k=0}^{p} \boldsymbol{A}(k)Y(n-k) + U(n)\ , \tag{1}$$

being $U(n) = [u_1(n)\ u_2(n)]^T$ a vector of zero-mean uncorrelated white noises with 2×2 diagonal covariance matrix $\boldsymbol{\Sigma} = \mathrm{diag}\{\sigma_1^2, \sigma_2^2\}$, and $\boldsymbol{A}(k)$ the 2×2 coefficient matrix in which the coefficient $a_{ij}(k)$ describes the interaction from $y_j(n-k)$ to $y_i(n)$ (*i,j*=1,2).

The estimated model coefficients are represented in the Z domain through the Z-transform of (1), thus yielding $Y(z) = \boldsymbol{H}(z)U(z)$, where the 2×2 transfer matrix is

$$\boldsymbol{H}(z) = \begin{bmatrix} H_{11}(z) & H_{12}(z) \\ H_{21}(z) & H_{22}(z) \end{bmatrix} = [\boldsymbol{I} - \boldsymbol{A}(z)]^{-1} = \bar{\boldsymbol{A}}(z)^{-1} , \qquad (2)$$

being $\boldsymbol{A}(z) = \sum_{k=1}^{p} \boldsymbol{A}(k) z^{-k}$ the coefficient matrix in the Z domain and $\boldsymbol{I}$ the 2×2 identity matrix. Taking the inverse of $\bar{\boldsymbol{A}}(z)$, each element of the transfer matrix is represented as follows (i,j=1,2; $i \neq j$)

$$H_{ii}(z) = \frac{\bar{A}_{jj}(z)}{|\bar{\boldsymbol{A}}(z)|}; \; H_{ij}(z) = \frac{-\bar{A}_{ij}(z)}{|\bar{\boldsymbol{A}}(z)|}. \qquad (3)$$

Computing $\boldsymbol{H}(z)$ on the unit circle in the complex plane ($\boldsymbol{H}(f) = \boldsymbol{H}(z)|_{z=e^{j2\pi f T_s}}$), the 2×2 spectral density matrix of the bivariate process in the frequency domain becomes $\boldsymbol{S}(f) = \boldsymbol{H}(f)\boldsymbol{\Sigma}\boldsymbol{H}^{*}(f)$, where * indicates the Hermitian transpose. In this matrix, the diagonal terms $S_{ii}(f)$ correspond to the auto-spectra, while the off-diagonal terms $S_{ij}(f)$ correspond to the cross-spectra.

From the frequency domain representation of the AR model, the diagonal elements of the spectral density matrix can be elaborated to estimate a non-causal measure of spectral gain from y_j to y_i $(i, j = 1,2, i \neq j)$:

$$G_{ij}^{\alpha}(f) \triangleq \sqrt{\frac{S_{ii}(f)}{S_{jj}(f)}} \qquad (4)$$

where the superscript α denotes the non-causal index first used by Pagani et al. [20]. The α measure is a non-causal index of gain, because its main assumption is that the whole variability of y_i is driven by y_j. To get a causal measure, first each auto-spectrum is expressed as the sum of causal contributions from Eqs. (2,3) to yield

$$S_i(f) \triangleq S_{ii}(f) = \sigma_i{}^2 |H_{ii}(f)|^2 + \sigma_j{}^2 |H_{ij}(f)|^2 , \qquad (5)$$

being $\sigma_j{}^2 |H_{ij}(f)|^2 \triangleq S_{i|j}(f)$ the partial spectrum of y_i given y_j (i,j=1,2). A left-side normalization of (5) produces $\gamma_{ii}{}^2(f) + \gamma_{ij}{}^2(f) = 1$, where

$$\gamma_{ij}^2(f) \triangleq \frac{\sigma_j{}^2 |H_{ij}(f)|^2}{S_{ii}(f)} = \frac{S_{i|j}(f)}{S_i(f)} \qquad (6)$$

is the squared directed (causal) coherence (DC) from y_j to y_i, a function assessing the normalized coupling strength from y_j to y_i in the frequency domain [19]. The DC ranges between 0 and 1, being 0 when y_j does not cause y_i at frequency f, and 1 when the whole power of y_i at frequency f is due to the variability of y_j [24]. The causal information conveyed in the DC allows to define a causal measure of spectral gain, first used by Faes et al. [10]:

$$G_{ij}^{\gamma}(f) \triangleq G_{ij}^{\alpha}(f) \gamma_{ij}^2(f) \qquad (7)$$

The γ measure (7) weights the power ratio defined in (4) through the causal coherence from y_j to y_i.

2.2 Measures of causal coupling and gain derived from causal spectral decomposition

The measures defined by Eqs. (4, 6, 7) are "frequency-specific" in the sense that they are computed at each frequency; therefore, when they have to be computed within a specific frequency band, an "overall" estimate is typically extracted as the average of that measure within the band. For this reason, these are referred to as "global measures" in the following. Nonetheless, such global values in the selected band can be misleading, being unable to objectively quantify the causal contribution of the source process to the power of the target one [22]. As an alternative, we herein propose "pole-specific" measures that can be related to the poles of the transfer function of the bivariate AR model. Their computation is associated to the pole frequency, and thus allows to get "local" measures of causal coupling or gain, where "local" is meant to indicate individual oscillations localized at specific frequencies. In the following, we define local measures of causal coupling (pole-specific spectral causality, PSSC [22]) and causal and non-causal local measures of gain (pole-specific spectral gain, PSSG) to assess in the frequency domain both the strength and the magnitude of the directed interactions between two processes.

Exploiting spectral decomposition [21], each transfer function defined as in (3) is decomposed as the sum of q spectral components ($q \cong p/2$), which correspond to the poles of the determinant of $\bar{\boldsymbol{A}}(z)$. Every spectral component is described by a specific profile and has an associated frequency (related to the pole phase) and power (related to the pole residual). In this way, the complex partial PSD of the i^{th} process given the j^{th} process, which can be written in the Z-domain as

$$S_{i|j}(z) = H_{ij}(z)\sigma_j^2 H_{ij}^*(1/z^*), \tag{8}$$

can be expanded decomposing the $i-j^{th}$ transfer function as

$$H_{ij}(z) = \frac{\bar{A}_{ij}(z)}{|\bar{\boldsymbol{A}}(z)|} = \frac{\bar{A}_{ij}(z)}{\prod_k (z-z_k)}, \tag{9}$$

being the poles z_k, $k=1,...q$ the roots of $|\bar{\boldsymbol{A}}(z)|$. The expansion of each partial spectrum in (8) is performed exploiting Heaviside decomposition with simple fractions relevant to all its poles (i.e., the poles z_k inside the unit circle and their reciprocals $\bar{z}_k = z_k^{-1}$ outside the unit circle, with $k=1,...,q$), which are fractions weighted by the relevant residuals of $S_{i|j}(z)$ (*i.e.*, $r_k z_k$ and $-r_k \bar{z}_k$), to get [21]

$$S_{i|j}(z) = \sum_{k=1}^{q} S_{i|j}{}^{(k)}(z),\ S_{i|j}{}^{(k)}(z) = \frac{r_k z_k}{z-z_k} - \frac{r_k \bar{z}_k}{z-\bar{z}_k}. \tag{10}$$

After extracting the residuals and expanding the partial spectrum in simple fractions and given that $S_i(z) = S_{i|i}(z) + S_{i|j}(z)$, we obtain the spectrum of y_i computing (10) for values of z on the unit circle of the complex plane [22]:

$$S_i(f) = \sum_{k=1}^{q} S_i^{(k)}(f) = \sum_{k=1}^{q} S_{i|i}^{(k)}(f) + S_{i|j}^{(k)}(f)\,. \tag{11}$$

The k^{th} spectral component $S_{i|j}^{(k)}(f)$, $i,j = 1{,}2$, has an associated frequency related to the pole phase, $f(k) = \arg\{z_k\}$, and power related to the pole residuals, $P_{i|j}(k) = r_k$ for real poles and $P_{i|j}(k) = r_k + r_k^*$ for complex conjugate poles. It is then possible to achieve a decomposition for the DC from y_j to y_i normalizing the spectral components to the total spectrum as follows:

$$\gamma_{ij}^2(f) = \sum_{k=0}^{q} \gamma_{ij}^{2(k)}(f), \quad \gamma_{ij}^{2(k)}(f) \triangleq \frac{S_{i|j}^{(k)}(f)}{S_i(f)}. \tag{12}$$

Furthermore, causal contributions to the spectral power can be obtained by integrating each spectral component over the whole frequency axis. This allows to exploit (11) for decomposing the variance of the process y_i, λ_i^2, as

$$\lambda_i^2 = \frac{2}{f_c}\int_0^{f_c} S_i(f)df = \sum_{k=0}^{q} P_{i|i}(k) + P_{i|j}(k) = \sum_{k=0}^{q} P_i(k) \quad (13)$$

where $P_{i|i}(k) = \int_0^{f_c} S_{i|i}^{(k)}(f)df$ is the part of the variance of y_i due to its own dynamics and relevant to k^{th} oscillation (pole), $P_{i|j}(k) = \int_0^{f_c} S_{i|j}^{(k)}(f)df$ is the part of the variance of y_i due to y_j and relevant to the k^{th} pole, and by summing these two contributions to the variance we get the part of the variance of y_i relevant to the k-th pole, *i.e*, $P_i(k) = P_{i|i}(k) + P_{i|j}(k)$. Using these partial variances, the PSSC relevant to the k^{th} oscillation is obtained as a local causal measure of coupling from y_j to y_i:

$$\gamma_{i|j}^2(k) \triangleq \frac{P_{i|j}(k)}{P_i(k)}\,. \tag{14}$$

The PSSC ranges between 0 and 1, being equal to 0 when the power of the k^{th} oscillation of y_i (*i.e.* the oscillation at frequency f_k) is totally due to its internal dynamics and equal to 1 when it is totally caused by the dynamics of y_j assessed at the same frequency f_k. Given that the frequency f_k is associated to a specific causal spectral profile, the corresponding PSSC value represents an objective measure of the causal power at that frequency, so that the total causal power in a specific frequency band f can be easily computed summing all PSSC values with frequency within that band. Using the same formalism, we also define a local non-causal measure of gain (local PSSG) from y_j to y_i related to the k^{th} pole as

$$G_{ij}^{\alpha}(k) \triangleq \sqrt{\frac{P_i(k)}{P_j(k)}}. \tag{15}$$

The gain measure defined in (15) relates the whole variability of the output process y_i to that of the input process y_j without attempting to separate causal and non-causal contributions. To get a causal measure, we consider only the power of y_i causally due to y_j and related to the k^{th} pole and define the local PSSG from y_j to y_i as:

$$G^{\gamma}_{i|j}(k) = \sqrt{\frac{P_{i|j}(k)}{P_j(k)}}. \tag{16}$$

Note that, while the spectral causality is an adimensional measure, the spectral gain is expressed in units of measurement of the output series divided by units of measurement of the input series.

2.3 *Computation in cardiovascular variability analysis*

To evaluate the new proposed local measures in comparison with the traditional global measures of both causal coupling and gain, the latter distinguishing also between causal and non-causal indices, we considered pairs of simultaneously observed beat-to-beat time series of SAP and RR, corresponding respectively to realizations of the processes y_1 and y_2. In the frequency domain analysis, the coupling and gain functions were evaluated within the LF band, ranging from $f^{LF}_{inf} = 0.04$ Hz to $f^{LF}_{sup} = 0.15$ Hz [25], in order to minimize the effects of non-baroreflex mechanisms on the assessed measures and especially to avoid the confounding effects of respiration on SAP and RR which are primarily confined in the HF band [14–18,25]. Accordingly, after computing the spectrum of RR and SAP as well as their partial spectra and decomposition, the global measures of causal coupling (6), non-causal gain (4) and causal gain (7) were averaged in the LF band to get the following indexes ($i, j = 1,2, i \neq j$):

- Global causal coupling: $\gamma^2_{ji}(LF) \triangleq \frac{1}{f^{LF}_{sup} - f^{LF}_{inf}} \int_{f^{LF}_{inf}}^{f^{LF}_{sup}} \gamma^2_{ji}(f)\, df$ (17)
- Global non-causal gain: $G^{\alpha}_{ji}(LF) \triangleq \frac{1}{f^{LF}_{sup} - f^{LF}_{inf}} \int_{f^{LF}_{inf}}^{f^{LF}_{sup}} G^{\alpha}_{ji}(f)\, df$ (18)
- Global causal gain: $G^{\gamma}_{ji}(LF) \triangleq \frac{1}{f^{LF}_{sup} - f^{LF}_{inf}} \int_{f^{LF}_{inf}}^{f^{LF}_{sup}} G^{\gamma}_{ji}(f)\, df.$ (19)

On the other hand, local band-specific measures were obtained applying the equations for causal coupling (14), non-causal gain (15) and causal gain (16) after summing the power content of all the components with central frequency f_k within the LF range, *i.e.* computing ($i, j = 1,2, i \neq j$):

- Local causal coupling: $\gamma^2_{j|i}(k_{LF}) = \frac{\sum_{f_k \in LF} P_{j|i}(k)}{\sum_{f_k \in LF} P_j(k)}$ (20)

- Local non-causal gain: $G_{ji}^{\alpha}(k_{LF}) = \sqrt{\frac{\sum_{f_k \in LF} P_j(k)}{\sum_{f_k \in LF} P_i(k)}}$ (21)
- Local causal gain: $G_{j|i}^{\gamma}(k_{LF}) = \sqrt{\frac{\sum_{f_k \in LF} P_{j|i}(k)}{\sum_{f_k \in LF} P_i(k)}}$. (22)

The derivation of the local measures of coupling and gain is illustrated in Fig. 1 for representative SAP and RR time series. For the same time series, the derivation of the local measures of coupling and gain is illustrated in Fig. 2.

2.4 Experimental protocol and data analysis

The study included 35 post-AMI patients (58.5 ± 10.2 yrs, 4 female), examined 10 ± 3 days after AMI, and two groups of healthy subjects, 19 young (25.0 ± 2.6 yrs, 9 female) and 12 old (63.1 ± 8.3 yrs, 9 female), all monitored in the resting supine position and in the 60° upright position reached after passive head-up tilt [7,26]. After recording ECG (Siemens Mingograph, hardware bandpass filter 0.3-1000Hz, lead II) and non-invasive finger arterial pressure (Ohmeda 2300; Englewood, CO), the beat-to-beat variability series of RR interval and SAP were measured on a beat-by-beat basis. Two stationary and artifact-free windows, each of ~5 min duration, corresponding to 300 beats, were then selected in correspondence with the two epochs of the test. All signals were filtered to avoid the effect of long-term trends on the data analysis, employing an autoregressive high-pass filter with zero phase. Further details on experimental protocol and data acquisition can be found in [7,26].

Each pair of RR and SAP series were fitted by a bivariate AR model, after allowing instantaneous zero-lag effects in the direction from SAP to RR, (i.e., setting $a_{21}(0) \neq 0$ and $a_{ij}(0) = 0$ as a constraint for model identification) to allow fast within-beat baroreflex influences in agreement with the adopted measurement convention. Model identification was performed via the vector least-squares approach, setting the model order p according to the multivariate version of the Akaike criterion [27]. In some cases, the use of the Akaike criterion led to negative power contributes and/or complex coupling and gain indices as a result of the residue theorem, which may have caused erroneous final results. To avoid such a problem, all the obtained results were manually checked and, in case of negative power contributions, the model order p was slightly varied and thus manually selected to achieve positive power values. After AR identification, estimation of the global and local measures of causal coupling and causal and non-causal gain were computed from the estimated model parameters as described in the previous sections. Spectral analysis was performed assuming the series as uniformly sampled with the mean heart period $\langle RR \rangle$ taken as the sampling period T_s, so that the Nyquist frequency in each spectral representation was taken as $\frac{f_s}{2} = \frac{1}{2\langle RR \rangle}$.

As regards the statistical analysis, the distributions of the coherence and gain indices were tested for normality using the Anderson-Darling test [28,29]. Since the hypothesis of normality was rejected for most of the distributions, and given the small sample size especially for young and old subjects, non-parametric tests were employed [30]. For any given group, the statistical significance of the difference between rest and tilt conditions was assessed using the Wilcoxon signed rank test [31]. Afterwards, the statistical significance of the differences of the median of the distributions among groups at a given physiological condition (rest or tilt) was assessed using the non-parametric Kruskal Wallis test [32]. When the null hypothesis that the data in each group comes from the same distribution was rejected, a pairwise comparison was carried out using the Dunn post-hoc test with Šidák correction for multiple comparisons (*n*=3) [33,34] to assess differences between group pairs (Young vs Old, Old vs AMI and Young vs AMI) at a given condition (rest or tilt). Finally, to assess the statistical differences between global and local or causal vs non-causal indices given the group and the condition, the Wilcoxon signed rank test [31] was employed. All statistical tests were carried out with 5% significance level.

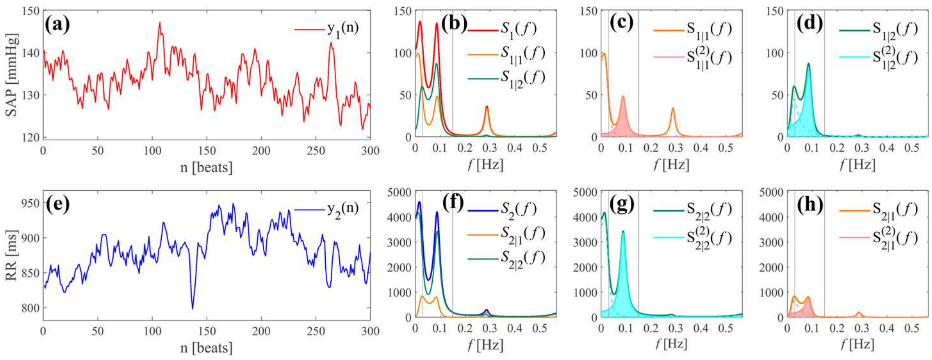

Figure 1. Example of causal spectral decomposition of the interactions between systolic arterial pressure (SAP) and heart period (RR intervals). (a) and (e): SAP and RR time series, respectively, for a representative AMI subject in the resting supine position. (b): the power spectrum of SAP is given by $S_1(f)$ and is decomposed as the sum of a causal spectrum $[S_{1|2}(f)]$ and a non-causal spectrum $[S_{1|1}(f)]$; (c) and (d): the non-causal (c) and causal (d) spectra of SAP are in turn decomposed with the spectral decomposition method into contributions associated to specific oscillations of the time series, with those in the LF band (pole *k*=2) given by $S_{1|1}^{(2)}(f)$ (non-causal part, c) and $S_{1|2}^{(2)}(f)$ (causal part, d). (f): the power spectrum of RR is given by $S_2(f)$ and is decomposed as the sum of a causal spectrum $[S_{2|1}(f)]$ and a non-causal spectrum $[S_{2|2}(f)]$; (g) and (h): the non-causal (g) and causal (h) spectra of RR are in turn decomposed into contributions associated to specific oscillations, with those in the LF band given by $S_{2|2}^{(2)}(f)$ (non-causal part, g) and $S_{2|1}^{(2)}(f)$ (causal part, h). Local measures are computed as follows: the PSSC from SAP to RR in the LF band, $\gamma_{21}^2(k_{LF})$, is computed as the ratio between the power $P_{2|1}^{(2)}(LF)$ (pink area, (h)) and the total power $P_{2|1}^{(2)}(LF) + P_{2|2}^{(2)}(LF)$ (pink + cyan areas, (h) and (g)); the non-causal PSSG from SAP to RR in the LF band, $G_{21}^{\alpha}(k_{LF})$, is computed as the squared root of the ratio between the total power $P_{2|1}^{(2)}(LF) + P_{2|2}^{(2)}(LF)$ (pink + cyan areas, (h) and (g)) and the total power $P_{1|2}^{(2)}(LF) + P_{1|1}^{(2)}(LF)$ (cyan + pink areas, (d) and (c)); the causal PSSG from SAP to RR in the LF band, $G_{21}^{\gamma}(k_{LF})$, is computed as the squared root of the ratio between the power $P_{2|1}^{(2)}(LF)$ (pink area, (h)) and the total power $P_{1|2}^{(2)}(LF) + P_{1|1}^{(2)}(LF)$ (cyan + pink areas, (d) and (c)). The same procedure applies to the computation of the directed coherence and gain indexes from RR to SAP.

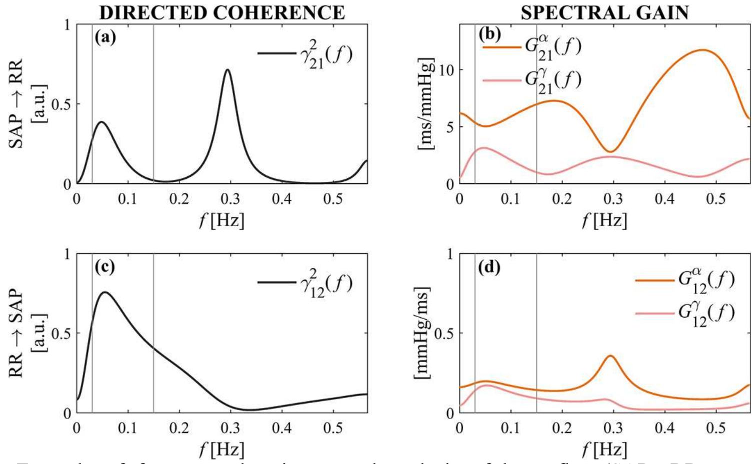

Figure 2. Example of frequency domain spectral analysis of baroreflex (SAP→RR, top row) and feedforward (RR→SAP, bottom row) interactions for a representative AMI subject in the resting supine position. (a) and (c): directed coherence function, $\gamma_{ij}^2(f)$ (*i,j=1,2* and *i≠j*); (b) and (d): spectral profiles of the non-causal gain $G_{ij}^{\alpha}(f)$ and of the causal gain $G_{ij}^{\gamma}(f)$ (*i,j=1,2* and *i≠j*). These 'frequency-specific' measures were averaged in the low frequency band (vertical grey lines in each plot) to get global measures.

3. Results

In this section, the results of LF spectral decomposition and analysis are reported, showing the distributions of the causal and non-causal indices described in Section 2, alongside with the outcomes of the statistical analyses carried out between different physiological conditions and between the various measures. The results in terms of causal coupling measures and of gain measures are depicted in Figures 3 and 4, respectively.

In the baroreflex direction from SAP to RR (Fig. 3, top panels), both global and local measures of causal coupling were significantly higher during tilt than during rest for all groups, showing a clear response to postural stress of the DC along the baroreflex. Moreover, while the global values were significantly lower in Old and AMI subjects compared with Young during both rest and tilt (Fig. 3a), the local index showed a significant decrease only in AMI compared with Young in both postural conditions (Fig. 3b).

As regards the gain measures in the same direction (Fig. 4, top panels) the non-causal indices decreased in Old compared to Young during postural stress, while they did not elicit striking differences relevant to the AMI group (Fig. 4a,c). On the contrary, the causal gain indices (measured both globally ad locally) detected a statistically significant decrease of the gain not only in Old, but also in AMI compared to Young, in both body positions (Fig. 4b,d). Moreover, the comparison between the two experimental conditions revealed that the gain index decreased significantly moving from rest to tilt in all the three groups if computed using the non-causal methods (Fig. 4a,c), only in AMI patients using the causal global method (Fig. 4b), and in none of the groups using the causal local method (Fig. 4d).

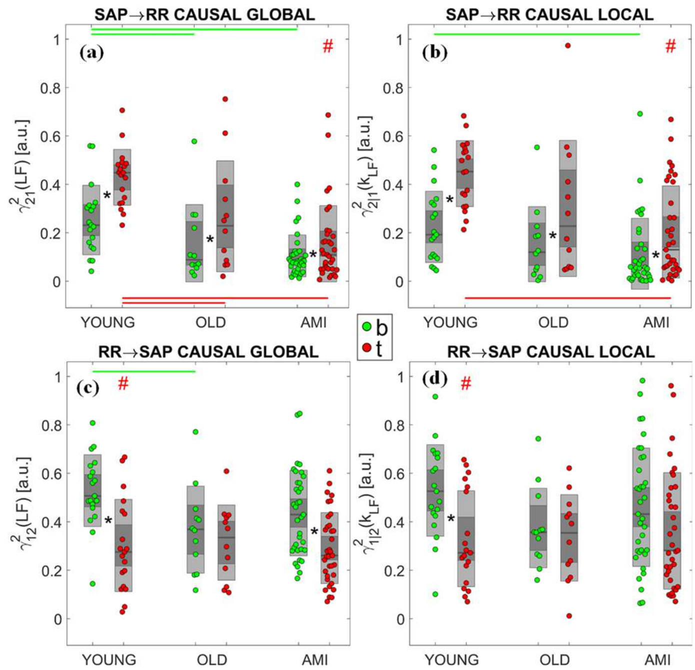

Figure 3. Results of low frequency (LF) spectral causality analysis of baroreflex (top row) and feedforward (bottom row) interactions based on the global and local directed (causal) coherence (respectively, $\gamma_{ij}^2(LF)$ and $\gamma_{ij}^2(k_{LF})$, where *i,j=SAP*, RR and *i≠j*). Plots depict the distributions across subjects, shown as individual values and box-plot distributions, of the directed coherence from SAP to RR and from RR to SAP, computed in the supine (green) and upright (red) body positions. Statistically significant differences: *, rest vs. tilt; #, global vs. local; −, YOUNG vs. OLD, YOUNG vs. AMI or OLD vs. AMI.

Global and local measures of coupling and gain were also investigated in the feedforward direction, where mechanical effects are known to alter RR variability according to changes in SAP variability [16]. The local measure of causal coupling decreased significantly from rest to tilt in Young but not in Old and AMI (Fig. 3d). The corresponding global measure of feedforward coupling decreased with tilt also in the AMI patients, and was lower in Old than in Young in the supine position (Fig. 3c). As regards the gain from RR to SAP, the non-causal measures (both global and local) were significantly higher during orthostatic stress in all three groups (Fig. 4e,g), while the causal global measure increased significantly in Old and AMI (Fig. 4f) and the causal local measure increased significantly only in AMI (Fig. 4h).

Figs. 3 and 4 illustrate also that non-causal measures of gain are always significantly lower than the corresponding causal ones, which is an obvious consequence of their mathematical formulation (i.e., the global causal gain (7) is obtained multiplying the global non-causal gain (4) by the DC, and the local causal gain (16) contains at the numerator a fraction of the power contained in the global non-causal gain (15)). Moreover, local measures tend to be lower in value than the corresponding global ones, being related to a specific oscillation in the LF band; the statistically significant differences in Fig. 4 are just a few, i.e. for Young (tilt and rest) and Old (tilt) in SAP→RR non causal index, for Young (rest) with regard to

SAP→RR causal index and for Young and AMI (tilt) causal index in RR→ SAP direction. Instead, comparing DC measures (Fig. 3), global and local indices resulted statistically different just for AMI tilt (SAP→RR direction) and for Young tilt (RR→SAP).

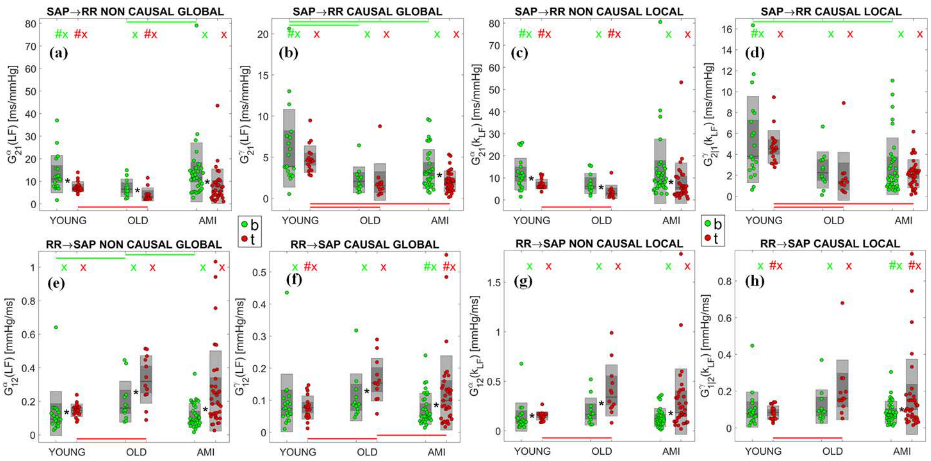

Figure 4. Distributions over subjects of the BRS computed in the LF band with the two different approaches (from left: non-causal and causal global measures, non-causal and causal local measures) along the two directions of interest (top: baroreflex direction from SAP to RR; bottom: feedforward direction from RR to SAP), in the rest (green) and tilt (red) phases of the testing protocol. Statistically significant differences: *, rest vs. tilt; #, global vs. local; −, YOUNG vs. OLD, YOUNG vs. AMI or OLD vs. AMI; *x*, non-causal vs. causal.

4. Discussion

Evaluation of the baroreflex gain is considered an important tool in clinical practice for diagnosis and prognosis in many cardiac diseases, including acute myocardial infarction [4–7,10,13]. A decreased baroreflex sensitivity has been already observed in several pathological conditions as a marker of cardiovascular system impairment [7,10,13]. In this study, we propose a new method to assess the BRS in the frequency domain, investigating the usefulness of using local causal measures (*i.e.* 'pole-specific' measures) in place of already widely employed global approaches (*i.e.* 'frequency-specific' measures); the comparison is extended to non-baroreflex (feedforward) interactions to investigate the relevant underlying mechanisms.

Causal methods have been already proved in the literature as useful tools, typically more reliable than non-causal ones, for the quantitative assessment of cardiovascular regulatory mechanisms [10,35,36]. Moreover, preliminary results have shown that the frequency-averaging approaches commonly undertaken to obtain an individual value from a spectral function (e.g., the DC) for evaluating it within a specific band of interest (e.g., the LF band) may be inaccurate as they can incorporate spectral contributions originating from neighboring frequency ranges [22]. In the following, we compare more thoroughly causal vs non-causal and local vs global indices to put in evidence strengths and drawbacks of each approach in light of our results.

4.1 Causal vs. non-causal assessment of cardiovascular interactions

In physiological conditions, RR and SAP normally reciprocally affect each other due to both regulatory feedback and mechanical feedforward coupling mechanisms (mainly of mechanical nature, such as the Windkessel and Frank-Starling effects) [23,36]. The presence of a closed-loop interaction between the heart period and the systolic arterial pressure highlighted by past works [2,23,36,37] suggests the importance to implement causality to assess cardiovascular interactions.

Our results confirm the findings already reported in the literature [10,35,36] highlighting the suitability of a causal (γ index) instead of a non-causal method (α index) for the frequency domain evaluation of BRS. The values of causal gain indices obtained in our analysis are significantly lower than the corresponding non-causal ones in all the groups of subjects during rest and head-up tilt. This finding confirms that the non-causal approach may overestimate the BRS, while closed-loop modeling allows to separately evaluate feedback and feedforward pathways, quantifying their relative contribution to the overall cardiovascular regulation [10].

The mixing between feedback and feedforward RR-SAP interactions can be also the reason why the non-causal measures of BRS detected a lower gain during postural stress not only in the AMI patients, but also in the Old and Young healthy subjects. The effect of tilt maneuver on the power spectrum of heart rate variability (HRV) is widely known [38–41], as is recognized that it evokes a greater effectiveness of the baroreflex that is mirrored by higher values of coupling between SAP and RR during postural stress; this effect was observed both in the present and in previous investigations [10,16,42]. Nevertheless, a decrease of the magnitude of the reflex, mirrored by the gain estimate, is more difficult to explain physiologically; here, the latter was observed only in the AMI patients using the global causal measure. Moreover, the causal measures of gain (both global and local) highlighted a significantly lower gain in the Old group, and especially in the AMI group, compared to the Young group. These decreased BRS values were observed in both the supine and upright position, documenting a reduced response of the baroreflex likely related to an impairment occurring with the coronary disease.

As regards the mechanical feedforward, the significant increase with head-up tilt observed for the non-causal measures of gain in all groups was found consistently for both causal measures only in the AMI patients. This result may be an indication of a physiological response to tilt that occurs as a consequence of the disease (as discussed in Sect 4.3), and is observed in young healthy subjects only when non-causal methods are improperly used to assess the gain function.

4.2 Global vs. local assessment of cardiovascular interactions

From a methodological point of view, the operation of averaging spectral functions (like the DC or the gain) to get a global index within an assigned frequency band could lead to inaccurate evaluation of the index, because external broadband oscillations may convey information into the analyzed band. This aspect, that we demonstrated recently in a theoretical example [22], is a major deal in cardiovascular variability analysis where VLF oscillations are often predominant and may thus have an impact on the evaluation of the DC or the BRS in the LF band of the spectrum [22]; a similar effect of spreading between adjacent bands may involve also the HRV oscillations located in the HF band and mainly due to respiration [14,25,38]. On the other hand, the method of spectral decomposition allows to focus more objectively on the spectral content within specific ranges, lastly resulting in DC and gain values (local measures) which are expected to reflect more accurately the underlying mechanisms of effectiveness and magnitude of a reflex with regard to the oscillations of physiological interest.

In the light of the methodological considerations above, we interpret the agreement often found between global and local measures as indicative of a limited impact of broadband VLF or HF spectral contributions into the analyzed LF band. This was the case, in the feedback direction from SAP to RR, for the significantly lower values of both causal coupling and gain observed in AMI compared to Young in both body positions and for the increase with tilt of the causal coupling in all groups, and, in the feedforward direction from RR to SAP, for the decrease in Young (but not in Old and AMI) of the causal coupling and the increase in AMI (but not in Young) of the causal gain observed moving from rest to tilt. These results, consistently found using both global and local causal measures, are interpreted as robust and are discussed physiologically in Sect. 4.3.

On the other hand, a disagreement between global and local measures of causal influence is likely indicating an effect of bands external to the LF on the global computation based on averaging. In our analysis, the main occurrence of this disagreement is the detection in AMI of a significant decrease of the causal gain from SAP to RR observed moving from rest to tilt with the global method but not with the local method; this suggests that, in the analysed post-infarction patients, a depressed BRS response to tilt occurs with contributions to cardiovascular variability located in frequency bands other than the LF. The other differences observed between the global and local approaches regard mostly comparisons involving the Old group; these may be explained also by the small size of this group (see Sect. 4.4).

4.3 Characterization of feedback and feedforward cardiovascular interactions via a local causal approach

As discussed in the previous subsections, the local causal method may be considered the methodologically most accurate approach for assessing the coupling and gain related to specific oscillations of the two analyzed time series, as it is able to separately evaluate feedback and feedforward pathways and to avoid confounding spectral contributions from other frequency ranges. In the analyzed data, the local causal approach showed a tendency to detect less statistically significant differences in the comparisons between groups and conditions; as these seem to be more conceivable and with a more robust physiological meaning, we discuss them from a physiological viewpoint.

Compared to the young heathy controls, a significantly lower causal coupling along the baroreflex direction from SAP to RR was detected in post-AMI patients during each of the two analyzed experimental conditions; the difference with Young was not statistically significant in the Old group when the local method was adopted to measure the causal coupling. This result is in agreement with previous findings in the literature which highlighted an overall lower synchronization index and an increase of the number of subjects showing uncoupled RR and SAP dynamics [7]. Moreover, the post-AMI patients showed also significantly an impaired baroreflex gain compared to the young subjects, both at rest and during tilt. This result, that was observed also in Old during tilt, can be attributed to the higher sympathetic tone of these subjects and to an inability to respond to changes in cardiac output by further sympathetic activation [7], and can be related to the known reduction of heart rate variability typically occurring in elderly and AMI subjects [43–45].

When the response to head-up tilt was analyzed, we observed in all groups a significant increase of the causal coupling along the baroreflex pathway moving from the supine to the upright position. This finding is typically related to the sympathetic activation produced by the postural stress induced by tilt [46,47] which has already been widely observed in the literature [38,39,41,48]. Overall, it reflects the increased effectiveness of the baroreflex in response to an orthostatic maneuver. The fact that it was observed also in the post-AMI patients, together with the observation that none of the groups denoted significant variations of the local causal gain moving from rest to tilt, seems to suggest that the baroreflex response to postural stress is preserved, in terms of increased effectiveness and unaltered sensitivity, after myocardial infarction. On the other hand, the statistically significant decrease of the global causal gain observed with tilt only in AMI patients points out a decreased BRS due to tilt, which agrees with previous findings indicating a reduced capability to cope with the postural challenge after AMI [7,43]. We hypothesize that the symptoms of orthostatic intolerance manifested after AMI are associated with fluctuations of RR and SAP which are not confined within the LF band of the spectrum.

Along the feedforward direction, a significant decrease of the causal coupling after head-up tilt was detected in Young subjects but not consistently in Old or post-AMI patients. In healthy subjects, a statistically significant decrease with tilt of the coupling from RR to SAP was reported using causal methods in the time domain [49], where it was investigated in terms of the cascade of interactions from RR to diastolic blood pressure (DBP) and then to SBP. Physiologically, this causal coupling is associated with the cardiac run-off, the Windkessel effect and the Frank-Starling law, according to which modifications of the heart period affect the end diastolic volume and then the strength of the systolic contraction [49,50]. The tilt-induced decrease of the effectiveness of the feedforward mechanism can be associated by the increased heart rate which limits the cardiac run-off and consequently the systolic contraction, but other mechanisms cannot be excluded as blood pressure variability is also due to variations in the sympathetic blood vessels control [36]. The lack of a consistent reduction with tilt of the feedforward coupling in Old and AMI patients could thus be associated to an impairment of these physiological mechanisms related to age and disease.

The feedforward gain was found to increase in Old and post-AMI patients after orthostatic stress. Since the occurrence of acute myocardial infarction is thought to be responsible of a significant stiffening of the cardiac muscle, and aging is associated with a stiffening of the vascular bed, these alterations might lead to an alteration of the mechanical effects which allow heart period to drive SAP variability during head-up tilt. A role may be also played by the neural autonomic control, with a larger reduction of heart rate variability compared to SAP variability in AMI patients. The feedforward gain was found to significantly increase with the postural stress also in Old compared to Young subjects. The alteration of the capability of RR to drive SAP variability reported in Old people during tilt suggests that also aging can be responsible for a modification of feedforward mechanisms of mechanical nature that characterize the interactions from the heart period to the systolic arterial pressure. Such results are in agreement with other findings reported in the literature [7] that highlighted an unbalanced RR-SAP regulation in old subjects with increased feedforward and decreased feedback mechanism.

4.4 Limitations and future studies

The present study has some limitations that should be taken into account. First of all, according to the study protocol [7], cardiovascular signals of the AMI group were recorded at predischarge time on patients in pharmacological washout. Only a small subgroup of very low-risk post-AMI patients able to support the suspension of β-blocker treatment without appreciable risk and no taking of antiarrhythmic drugs was involved in the study. Therefore, the results of our study cannot be generalized to the general post-AMI population. Nonetheless, residual effects of the treatment with betablockers may still be present in the AMI patients and thus affect the analyzed cardiovascular dynamics [26].

Other limitations are related to the small sample size of Young (19 subjects) and especially Old (12 subjects) groups, and to the fact that such groups are not homogeneous in the gender distribution (males are prevalent in AMI, females are prevalent in Old, while the gender is balanced in Young) [26].

A methodological limitation consists in the selection of the order of the parametric model used to fit the time series. Model order selection is an issue in real data analyses, where the true order is usually unknown. A correct model order assessment is rather difficult because the estimated order may not meet the user expectations (in terms of spectral resolution when it is too low, or in terms of interpretability of highly variable spectral profiles when it is too high). In the present study, the use of the Akaike Information Criterion [27] for model order selection led sometimes to spectral contributes of difficult interpretation or even negative power values after spectral decomposition. For this reason, the manual selection of the model order p could represent a possible workaround to avoid negative power contributes and to obtain a better spectral representation in LF band, still maintaining a tradeoff between good data resolution and reasonably low model complexity.

Future activities may also include further studies on larger groups of subjects, or on patients affected by different pathologies (e.g. hypertension [51,52] or atherosclerosis [53,54]). Moreover, an improvement of the automatic order selection algorithm to avoid negative power values or the application of other criteria (e.g. Bayesian Information Criterion) may be envisaged [55].

5. Conclusion

This study emphasizes the importance of combining the novel method of spectral decomposition [21,56] and a causal approach to cross-spectral analysis [10,13] to investigate the coupling and gain mechanisms underlying the closed-loop cardiovascular regulation in healthy and diseased stats. Combining such approaches allows to quantify objectively, at specific well-defined frequencies, the causal contribution of SAP to RR along the baroreflex pathway and of RR to SAP along the mechanical feedforward. The application of the proposed method to cardiovascular time series of Young, Old and AMI subjects highlighted that causal local measures perform better than traditional non-causal approaches in the evaluation of BRS, suggesting that aging and infarction generate impairment of BRS occurring at rest and when carrying out the orthostatic maneuver.

These findings support the concept that the use of a spectral decomposition approach as well as the implementation of causality in the study of interactions between heart rate and arterial pressure allows to mitigate the confounding effects of other variables operating at different frequencies and of reverse-side mechanisms and is thus essential to achieve a more accurate BRS assessment in physio-pathological states and different postural conditions.

CRediT authorship contribution statement

Riccardo Pernice: Methodology, Software, Visualization, Writing-Original draft preparation. **Laura Sparacino:** Software, Visualization, Writing-Original draft preparation. **Giandomenico Nollo**: Data curation. **Alessandro Busacca**: Writing-Reviewing and Editing**. Luca Faes:** Methodology, Formal analysis, Validation, Writing- Reviewing and Editing, Supervision

Funding

R.P. is supported by the Italian MIUR PON R&I 2014-2020 AIM project no. AIM1851228-2. L.F. is supported by the Italian MIUR PRIN 2017 project 2017WZFTZP “Stochastic forecasting in complex systems”.

References

[1] R. Barbieri, G. Parati, J.P. Saul, Closed-versus open-loop assessment of heart rate baroreflex, IEEE Eng. Med. Biol. Mag. 20 (2001) 33–42.

[2] G. Parati, P. Castiglioni, A. Faini, M. Di Rienzo, G. Mancia, R. Barbieri, J.P. Saul, Closed-Loop cardiovascular interactions and the baroreflex cardiac arm: modulations over the 24 h and the effect of hypertension, Front. Physiol. 10 (2019) 477.

[3] T. Zanotto, T.H. Mercer, M.L. van der Linden, J.P. Traynor, C.J. Petrie, A. Doyle, K. Chalmers, N. Allan, J. Price, H. Oun, Baroreflex function, haemodynamic responses to an orthostatic challenge, and falls in haemodialysis patients, PLoS One. 13 (2018) e0208127.

[4] M.T. La Rovere, G.D. Pinna, G. Raczak, Baroreflex sensitivity: measurement and clinical implications, Ann. Noninvasive Electrocardiol. 13 (2008) 191–207.

[5] T. Yasumasu, G.A. Reyes del Paso, K. Takahara, Y. Nakashima, Reduced baroreflex cardiac sensitivity predicts increased cognitive performance, Psychophysiology. 43 (2006) 41–45.

[6] G.A. Reyes Del Paso, M.I. González, J.A. Hernández, S. Duschek, N. Gutierrez, Tonic blood pressure modulates the relationship between baroreceptor cardiac reflex sensitivity and cognitive performance, Psychophysiology. 46 (2009) 932–938.

[7] G. Nollo, L. Faes, A. Porta, B. Pellegrini, F. Ravelli, M. Del Greco, M. Disertori, R. Antolini, Evidence of unbalanced regulatory mechanism of heart rate and systolic pressure after acute myocardial infarction, Am. J. Physiol. - Hear. Circ. Physiol. 283 (2002) 1200–1207. https://doi.org/10.1152/ajpheart.00882.2001.

[8] G.M. De Ferrari, A. Sanzo, A. Bertoletti, G. Specchia, E. Vanoli, P.J. Schwartz, Baroreflex sensitivity predicts long-term cardiovascular mortality

after myocardial infarction even in patients with preserved left ventricular function, J. Am. Coll. Cardiol. 50 (2007) 2285–2290.

[9] T.G. Farrell, O. Odemuyiwa, Y. Bashir, T.R. Cripps, M. Malik, D.E. Ward, A.J. Camm, Prognostic value of baroreflex sensitivity testing after acute myocardial infarction., Heart. 67 (1992) 129–137.

[10] L. Faes, M. Masè, G. Nollo, K.H. Chon, J.P. Florian, Measuring postural-related changes of spontaneous baroreflex sensitivity after repeated long-duration diving: Frequency domain approaches, Auton. Neurosci. Basic Clin. 178 (2013) 96–102. https://doi.org/10.1016/j.autneu.2013.03.006.

[11] J. Krohova, L. Faes, B. Czippelova, R. Pernice, Z. Turianikova, R. Wiszt, N. Mazgutova, A. Busacca, M. Javorka, Vascular resistance arm of the baroreflex: Methodology and comparison with the cardiac chronotropic arm, J. Appl. Physiol. 128 (2020) 1310–1320. https://doi.org/10.1152/japplphysiol.00512.2019.

[12] E.E. Benarroch, The arterial baroreflex: functional organization and involvement in neurologic disease, Neurology. 71 (2008) 1733–1738.

[13] L. Sparacino, R. Pernice, G. Nollo, L. Faes, Causal and Non-Causal Frequency Domain Assessment of Spontaneous Baroreflex Sensitivity after Myocardial Infarction, in: 2020 11th Conf. Eur. Study Gr. Cardiovasc. Oscil., IEEE, 2020: pp. 1–2.

[14] J. Krohova, L. Faes, B. Czippelova, Z. Turianikova, N. Mazgutova, R. Pernice, A. Busacca, D. Marinazzo, S. Stramaglia, M. Javorka, Multiscale Information Decomposition Dissects Control Mechanisms of Heart Rate Variability at Rest and During Physiological Stress, Entropy . 21 (2019). https://doi.org/10.3390/e21050526.

[15] M. Javorka, J. Krohova, B. Czippelova, Z. Turianikova, N. Mazgutova, R. Wiszt, M. Ciljakova, D. Cernochova, R. Pernice, A. Busacca, L. Faes, Respiratory Sinus Arrhythmia Mechanisms in Young Obese Subjects, Front. Neurosci. 14 (2020) 204. https://doi.org/10.3389/fnins.2020.00204.

[16] L. Faes, G. Nollo, A. Porta, Mechanisms of causal interaction between short-term RR interval and systolic arterial pressure oscillations during orthostatic challenge, J. Appl. Physiol. 114 (2013) 1657–1667.

[17] F. Rahman, S. Pechnik, D. Gross, L. Sewell, D.S. Goldstein, Low frequency power of heart rate variability reflects baroreflex function, not cardiac sympathetic innervation, Clin. Auton. Res. 21 (2011) 133–141.

[18] D.S. Goldstein, O. Bentho, M. Park, Y. Sharabi, Low-frequency power of heart rate variability is not a measure of cardiac sympathetic tone but may be a measure of modulation of cardiac autonomic outflows by baroreflexes, Exp. Physiol. 96 (2011) 1255–1261.

[19] A. Porta, R. Furlan, O. Rimoldi, M. Pagani, A. Malliani, P. Van De Borne, Quantifying the strength of the linear causal coupling in closed loop interacting cardiovascular variability signals, Biol. Cybern. 86 (2002) 241–251.

[20] M. Pagani, V. Somers, R. Furlan, S. Dell'Orto, J. Conway, G. Baselli, S. Cerutti, P. Sleight, A. Malliani, Changes in autonomic regulation induced by physical training in mild hypertension., Hypertension. 12 (1988) 600–610.

[21] G. Baselli, A. Porta, O. Rimoldi, M. Pagani, S. Cerutti, Spectral decomposition in multichannel recordings based on multivariate parametric identification, IEEE Trans. Biomed. Eng. 44 (1997) 1092–1101. https://doi.org/10.1109/10.641336.

[22] L. Faes, J. Krohova, R. Pernice, A. Busacca, M. Javorka, A new Frequency Domain Measure of Causality based on Partial Spectral Decomposition of Autoregressive Processes and its Application to Cardiovascular Interactions*, in: 2019 41st Annu. Int. Conf. IEEE Eng. Med. Biol. Soc., 2019: pp. 4258–4261. https://doi.org/10.1109/EMBC.2019.8857312.

[23] G. Nollo, L. Faes, A. Porta, R. Antolini, F. Ravelli, Exploring directionality in spontaneous heart period and systolic pressure variability interactions in humans: implications in the evaluation of baroreflex gain, Am. J. Physiol.

Circ. Physiol. 288 (2005) H1777–H1785. https://doi.org/10.1152/ajpheart.00594.2004.

[24] L. Faes, S. Erla, G. Nollo, Measuring connectivity in linear multivariate processes: definitions, interpretation, and practical analysis, Comput. Math. Methods Med. 2012 (2012).

[25] F. Shaffer, J.P. Ginsberg, An Overview of Heart Rate Variability Metrics and Norms, Front. Public Heal. 5 (2017) 258. https://doi.org/10.3389/fpubh.2017.00258.

[26] L. Faes, M. Gómez-Extremera, R. Pernice, P. Carpena, G. Nollo, A. Porta, P. Bernaola-Galván, Comparison of methods for the assessment of nonlinearity in short-term heart rate variability under different physiopathological states, Chaos An Interdiscip. J. Nonlinear Sci. 29 (2019) 123114. https://doi.org/10.1063/1.5115506.

[27] H. Akaike, A new look at the statistical model identification, IEEE Trans. Automat. Contr. 19 (1974) 716–723.

[28] T.W. Anderson, D.A. Darling, Asymptotic theory of certain" goodness of fit" criteria based on stochastic processes, Ann. Math. Stat. 23 (1952) 193–212.

[29] B.W. Yap, C.H. Sim, Comparisons of various types of normality tests, J. Stat. Comput. Simul. 81 (2011) 2141–2155.

[30] A.K. Dwivedi, I. Mallawaarachchi, L.A. Alvarado, Analysis of small sample size studies using nonparametric bootstrap test with pooled resampling method, Stat. Med. 36 (2017) 2187–2205.

[31] J.D. Gibbons, S. Chakraborti, Nonparametric Statistical Inference: Revised and Expanded, CRC press, 2014.

[32] J.H. McDonald, Handbook of biological statistics, 2009.

[33] S.S. Sawilowsky, Real data analysis, IAP, 2007.

[34] Z. Šidák, Rectangular confidence regions for the means of multivariate normal distributions, J. Am. Stat. Assoc. 62 (1967) 626–633.

[35] L. Faes, A. Porta, R. Cucino, S. Cerutti, R. Antolini, G. Nollo, Causal transfer function analysis to describe closed loop interactions between cardiovascular and cardiorespiratory variability signals, Biol. Cybern. 90 (2004) 390–399.

[36] M. Javorka, B. Czippelova, Z. Turianikova, Z. Lazarova, I. Tonhajzerova, L. Faes, Causal analysis of short-term cardiovascular variability: state-dependent contribution of feedback and feedforward mechanisms, Med. Biol. Eng. Comput. 55 (2017) 179–190.

[37] A. Porta, G. Baselli, O. Rimoldi, A. Malliani, M. Pagani, Assessing baroreflex gain from spontaneous variability in conscious dogs: role of causality and respiration, Am. J. Physiol. Circ. Physiol. 279 (2000) H2558–H2567.

[38] R. Pernice, M. Javorka, J. Krohova, B. Czippelova, Z. Turianikova, A. Busacca, L. Faes, Reliability of Short-Term Heart Rate Variability Indexes Assessed through Photoplethysmography, in: 2018 40th Annu. Int. Conf. IEEE Eng. Med. Biol. Soc., 2018: pp. 5610–5613. https://doi.org/10.1109/EMBC.2018.8513634.

[39] R. Pernice, M. Javorka, J. Krohova, B. Czippelova, Z. Turianikova, A. Busacca, L. Faes, Comparison of short-term heart rate variability indexes evaluated through electrocardiographic and continuous blood pressure monitoring, Med. Biol. Eng. Comput. 57 (2019) 1247–1263. https://doi.org/10.1007/s11517-019-01957-4.

[40] A. Porta, E. Tobaldini, S. Guzzetti, R. Furlan, N. Montano, T. Gnecchi-Ruscone, Assessment of cardiac autonomic modulation during graded head-up tilt by symbolic analysis of heart rate variability, Am. J. Physiol. Circ. Physiol. 293 (2007) H702–H708. https://doi.org/10.1152/ajpheart.00006.2007.

[41] N. Montano, T.G. Ruscone, A. Porta, F. Lombardi, M. Pagani, A. Malliani, Power spectrum analysis of heart rate variability to assess the changes in sympathovagal balance during graded orthostatic tilt., Circulation. 90 (1994) 1826–1831.

[42] M. Di Rienzo, G. Parati, P. Castiglioni, R. Tordi, G. Mancia, A. Pedotti, Baroreflex effectiveness index: an additional measure of baroreflex control of heart rate in daily life, Am. J. Physiol. Integr. Comp. Physiol. 280 (2001) R744–R751.

[43] F. Lombardi, G. Sandrone, S. Pernpruner, R. Sala, M. Garimoldi, S. Cerutti, G. Baselli, M. Pagani, A. Malliani, Heart rate variability as an index of sympathovagal interaction after acute myocardial infarction, Am. J. Cardiol. 60 (1987) 1239–1245.

[44] R.E. Kleiger, J.P. Miller, J.T. Bigger Jr, A.J. Moss, Decreased heart rate variability and its association with increased mortality after acute myocardial infarction, Am. J. Cardiol. 59 (1987) 256–262.

[45] H. Tsuji, F.J. Venditti Jr, E.S. Manders, J.C. Evans, M.G. Larson, C.L. Feldman, D. Levy, Reduced heart rate variability and mortality risk in an elderly cohort. The Framingham Heart Study., Circulation. 90 (1994) 878–883.

[46] D.D. O'leary, D.S. Kimmerly, A.D. Cechetto, J.K. Shoemaker, Differential effect of head-up tilt on cardiovagal and sympathetic baroreflex sensitivity in humans, Exp. Physiol. 88 (2003) 769–774.

[47] W.H. Cooke, J.B. Hoag, A.A. Crossman, T.A. Kuusela, K.U.O. Tahvanainen, D.L. Eckberg, Human responses to upright tilt: a window on central autonomic integration, J. Physiol. 517 (1999) 617–628.

[48] A. Porta, T. Gnecchi-Ruscone, E. Tobaldini, S. Guzzetti, R. Furlan, N. Montano, Progressive decrease of heart period variability entropy-based complexity during graded head-up tilt, J. Appl. Physiol. 103 (2007) 1143–1149. https://doi.org/10.1152/japplphysiol.00293.2007.

[49] M. Javorka, J. Krohova, B. Czippelova, Z. Turianikova, Z. Lazarova, K. Javorka, L. Faes, Basic cardiovascular variability signals: mutual directed interactions explored in the information domain, Physiol. Meas. 38 (2017) 877–894. https://doi.org/10.1088/1361-6579/aa5b77.

[50] N. Westerhof, J.-W. Lankhaar, B.E. Westerhof, The arterial windkessel, Med. Biol. Eng. Comput. 47 (2009) 131–141.

[51] G. Grassi, F.Q. Trevano, G. Seravalle, F. Scopelliti, G. Mancia, Baroreflex function in hypertension: consequences for antihypertensive therapy, Prog. Cardiovasc. Dis. 48 (2006) 407–415.

[52] A. Berdeaux, J.F. Giudicelli, Antihypertensive drugs and baroreceptor reflex control of heart rate and blood pressure, Fundam. Clin. Pharmacol. 1 (1987) 257–282.

[53] N. Nasr, A. Pavy-Le Traon, V. Larrue, Baroreflex sensitivity is impaired in bilateral carotid atherosclerosis, Stroke. 36 (2005) 1891–1895.

[54] S. Simula, T. Laitinen, E. Vanninen, P. Pajunen, M. Syvänne, A. Hedman, J. Hartikainen, Baroreflex sensitivity in asymptomatic coronary atherosclerosis, Clin. Physiol. Funct. Imaging. 33 (2013) 70–74.

[55] A.A. Neath, J.E. Cavanaugh, The Bayesian information criterion: background, derivation, and applications, Wiley Interdiscip. Rev. Comput. Stat. 4 (2012) 199–203.

[56] L.H. Zetterberg, Estimation of parameters for a linear difference equation with application to EEG analysis, Math. Biosci. 5 (1969) 227–275. https://doi.org/https://doi.org/10.1016/0025-5564(69)90044-3.